Journal of
Materials Chemistry C

Accepted Manuscript

This article can be cited before page numbers have been issued, to do this please use: J. Garcia, V. M. Prida, L. G. Vivas, B. Hernando, E. Diaz Barriga Castro, R. Mendoza, C. Luna, J. Escrig and M. vazquez, *J. Mater. Chem. C*, 2015, DOI: 10.1039/C4TC02988G.

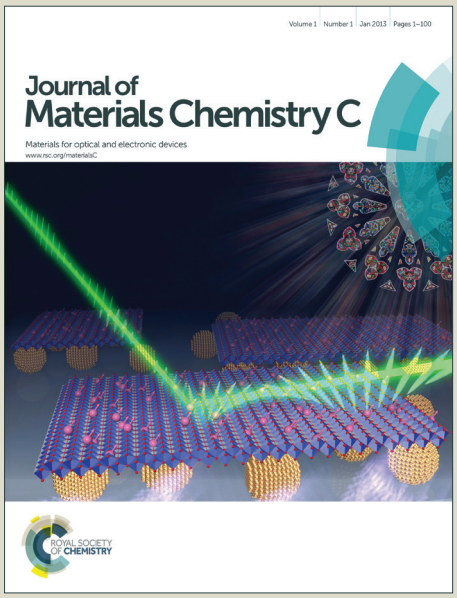

ROYAL SOCIETY OF CHEMISTRY

www.rsc.org/materialsC

View Article Online
DOI: 10.1039/C4TC02988G

Journal Name

RSCPublishing

ARTICLE

Cite this: DOI: 10.1039/xoxxoooooox

Magnetization Reversal Dependence on Effective Magnetic Anisotropy in Electroplated Co-Cu Nanowire Arrays

J. García [a], V. M. Prida [a], L. G. Vivas [b], B. Hernando [a], E. D. Barriga-Castro [c], R. Mendoza-Reséndez [d], C. Luna [c], J. Escrig [e], M. Vázquez [b]

Received ooth January 2012,
Accepted ooth January 2012

DOI: 10.1039/xoxxoooooox

www.rsc.org/

Arrays of $Co_{(100-x)}Cu_{(x)}$ ($0 \leq x \leq 27$) nanowires with 45 nm of diameter and 18 μm in length, have been potentiostatically electrodeposited into the hexagonally self-assembled nanopores of anodic alumina membranes. The structural characterization of Co-Cu nanowires confirms the coexistence of both *hcp* and *fcc* crystalline phases, with textures that are strongly affected by the fractional content of Cu. Parallel magnetic studies of the room temperature magnetization process by First Order Reversal Curve (FORC) analysis and the angular dependence of coercivity, confirm the presence of two coexisting ferromagnetic phases at intermediate Cu content nanowires, ascribed to a softer magnetic phase for pure Co and a harder magnetic one for the Co-Cu composition alloy, respectively. The temperature dependence of coercivity and remanence reveal a reorientation of the effective magnetic anisotropy with adding Cu into the Co-Cu alloy nanowires, being enhanced by the coexistence of the two ferromagnetic phases.

Introduction

The study of cylindrical magnetic nanowires is recently attracting much interest in view of their particular magnetic behavior as alternative to lithography nanostripes. The cylindrical symmetry determines specific local spin configuration with vortex like structure around the axis and consequently specific magnetization reversal process by domain walls motion[1,2]. Arrays of nanowires are customarily grown by electrochemical deposition into self-assembled nanoporous channels of anodic aluminum membranes employed as templates. That electrochemical route is a reliable method to fabricate high-quality ordered arrays of magnetic nanowires at low cost. In particular for this work, the well-defined spatial ordering of the alumina nanochanels provides a constant distance among the electrodeposited nanowires into the array that is of great relevance for the magnetic characterization of the own nanowire array, in order to extract the contribution of the magnetostatic interactions. In addition, this family of nanowires are being proposed as alternative in advanced technological applications, as in magnetic data storage devices, spin based shift registers and in a wide range of magnetic sensors[3,4].

Co nanowire arrays are currently investigated in view of the feasibility to tailor the magnetocrystalline anisotropy. Most commonly Co nanowires exhibit hexagonal close-packed (*hcp*) crystalline structure, and alternatively face-centered cubic (*fcc*) symmetry[5]. Both, the specific crystalline structure and in case, the c-axis of the *hcp* phase, can be tailored by controlling the electroplating parameters (pore diameter and the length of the nanowires, pH, current density or temperature of the electrolyte)[6-8]. The *hcp* phase presents strong uniaxial magnetocrystalline anisotropy which is partially balanced by the shape anisotropy when their magnetization easy axes are not collinear. In turn, the *fcc* phase exhibits a reduced magnetocrystalline anisotropy which is typically overcome by the shape anisotropy.

The structure can be alternatively tuned by alloying Co with magnetic and/or non-magnetic elements, which can improve the magnetic properties[9]. Co-Fe and Co-Ni alloy nanowire arrays, among others systems, have been intensively studied recently where the main crystalline phase is tailored by properly adjusting the relative composition of magnetic elements in the alloy, thus modifying the magnetic behavior[10,11].

The introduction of a limited content of non-magnetic element can give rise to significant modification of the magnetic behavior and its temperature dependence while it does not reduce significantly the magnetic induction. Particularly, the magnetic behavior of Co-Cu compounds depends on the specific elements content as well as the fabrication procedure (i.e., mechanical alloying, rapid solidification) and eventual alloying degree. In principle, Co-Cu elements form a granular system since Co and Cu are poorly miscible[12]. In Cu-rich

View Article Online
DOI: 10.1039/C4TC02988G
Journal Name

compositions, Co forms ferromagnetic clusters embedded in a non-magnetic conductive matrix which makes this system interesting for specific applications (i.e., based on giant magneto-resistance effect)[13,14]. The electrochemical route has been found to be a reliable technique to produce Co-Cu solid solutions, where some Co sites are substituted by Cu atoms forming a miscible alloyed material[15-16]. However, depending on the specific electrochemical deposition conditions employed during the nanowires growth, rather different composition, crystalline structure and magnetic behavior can be obtained for nanowire arrays of the same starting alloy[17]. In addition, there is a current trend to produce multilayered and multisegmented ferromagnetic systems with Cu spacers from a single electrochemical bath[18-25]. The incorporation of a small fraction of Cu into the ferromagnetic layer and/or segment cannot be avoided. For a deeper understanding of such complex nanostructures, the effect of small Cu addition into a ferromagnetic material must be carefully investigated. The distortion of the Co lattice introduced by the addition of Cu becomes a suitable tool to tune the structure and consequently the magnetic behavior[26-28]. Moreover, we should emphasize that the phase diagram for Co-Cu nanowires can differ from that of bulk material due to dynamical effects occurred during the electrodeposition procedure, nanoscale sized and confined growth inside the pores of anodic aluminum membranes.

Regarding the magnetic anisotropy of Co nanowire arrays and their temperature dependence two alternative interpretations are proposed in the literature. In one hand, the magnetoelastic anisotropy energy contribution can play an important role since the nanowires are embedded into the alumina pores and consequently submitted to mechanical stresses[29]. This fact can be especially manifested when measuring at different temperatures due to strain introduced by the different thermal expansion coefficients of metal and surrounding ceramic alumina[30], as well as by the non-oxidized Al remaining at the bottom of the alumina membrane[31]. Alternatively, the temperature variation of the magnetocrystalline anisotropy, particularly which of the *hcp* phase, can plays a relevant role to determine a reorientation of the effective magnetic anisotropy[32]. We should underline that both contributions depend on the particular crystalline structure, i.e. *fcc* and *hcp* Co phases. Thus, the study of the temperature dependence of magnetic properties supplies relevant information on the different magnetic phases that can form part of the material.

The magnetization process is commonly analyzed through the hysteresis loops and their parameters. Among other specific techniques, first order reversal curves (FORC) and the angular dependence of coercivity have been proved to be very valuable tools to interpret the magnetization reversal mechanism and the magnetic interactions in arrays of magnetic nanowires.

The objective of this investigation has been to determine the effects introduced by the addition of a limited amount of Cu into the Co-Cu alloy nanowires over the structural and magnetic properties. Arrays of Co-Cu nanowires with composition ranging from 0 up to 27 at.% of Cu have been investigated. In the present contribution, we show the results corresponding to three samples with the amount of Cu content ranging between 0 and 27 wt.%, whose properties are representative of those of the Co-Cu nanowires as the amount of Cu content in the alloy is varied in the aforementioned compositional range. After their synthesis by electrochemical route, morphological and structural analyses have been carried out through scanning electron microscopy, SEM, transmission electron microscopy, TEM, selected area electron diffraction, SAED, and X-ray diffraction, XRD, techniques.

The role played by Cu in the magnetization reversal characteristics has been first analyzed by the hysteresis loops and particularly through the angular dependence of the coercivity mechanism as well as through the analysis of first order reversal curves, FORC. The temperature dependence of the magnetization reversal is further investigated, which has led us to detect the reorientation of the effective magnetic anisotropy that is strongly modified by the amount of Cu present in the Co-Cu alloy nanowires.

Samples preparation, structure and compositional characterization

Synthesis of Co-Cu nanowires by template-assisted electrodeposition

Porous anodic aluminum membranes, PAAM, used as templates have been prepared by the well-known two step anodization method[33], starting from a high-purity aluminum foil (Al 99.999% Goodfellow) and employing 0.3M oxalic acid as electrolythic bath under a potentiostatic anodization voltage of $40V_{dc}$ at 3 ºC. Under these conditions, the typical values of pore diameter, D_p, and inter-pore distance, D_{int}, are around 40 nm and 105 nm, respectively, resulting in a porosity of around 10%. The remaining un-oxidized Al at the bottom substrate was then removed by selective chemical etching in an aqueous solution of Copper (II) Chloride (0.14 M) and Hydrochloric acid (10.75 M). Also, the residual alumina barrier layer that occludes the bottom of each pore was removed using Reactive Ion Etching (RIE) from the backside of the alumina templates in plasma generated from a mixture of O_2 and CF_4 at 12 mTorr under an applied power of 250 W. Finally, a thin Au layer was sputtered onto the back open porous alumina membrane, and subsequently electrodeposited from a commercial gold-plating solution (Orosene 999), in order to grow a Au metallic contact of around 1µm in thickness for the final electroplating process.

Then, the pores of the PAAM were filled by controlled electrochemical deposition. Pure Co nanowires were electrodeposited from a Watts-type electrolyte, which consists of 1.07M $CoSO_4 \cdot 7H_2O$ + 0.19M $CoCl_2 \cdot 6H_2O$ + 0.73M H_3BO_3, maintaining the pH = 4 and the temperature at 45ºC, to avoid the boric acid precipitation. In the case of Co-Cu nanowires, 0.04M $CuSO_4$ as Cu^{2+} ions source was added to the previous electrolyte. Three different samples have been prepared by varying the deposition voltages between -0.75V and -1.0V for $Co_{73}Cu_{27}$ and $Co_{92}Cu_8$ alloys, respectively, and -1V for pure Co nanowire arrays, measured versus an Ag/AgCl reference

Journal Name

View Article Online
DOI: 10.1039/C4TC02988G

electrode. The potentiostatic electrodeposition was carried out for 10 min in all the cases, in order to obtain high aspect ratio nanowires with about tens of μm in length.

Morphological and compositional characterization.

Morphology, microstructure and composition analysis of samples was performed using a Scanning Electron Microscope (SEM, JEOL 6100) equipped with an Energy Dispersive X-ray microanalysis system (EDS, Inca Energy 200). The high quality of PAAMs, the parallel alignment and morphology of electrodeposited nanowires can be appreciated in the SEM top and cross section views shown in Figures 1 a) and b). From SEM top-view images, an average nanopore and thus nanowire diameter of around 40 nm has been estimated. The length of nanowires as determined by SEM is in the range 13 to 18 μm. EDS analysis enabled to determine the composition of the $Co_{(100-x)}Cu_x$ alloy nanowires with an estimated error of around 1-2 %. This analysis have revealed the dependence of Cu concentration with the electrodeposition potential from $Co_{73}Cu_{27}$ (-0.75V vs Ag/AgCl) to $Co_{92}Cu_8$ (-1V vs Ag/AgCl).

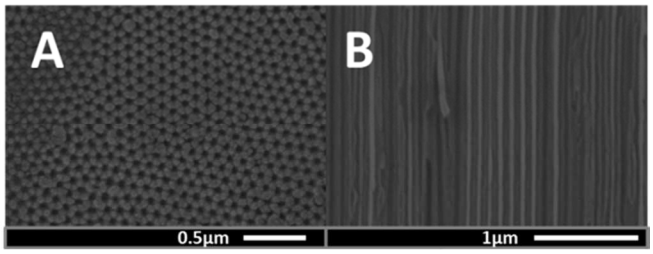

Figure 1: *SEM images: top-view of a typical nanoporous alumina membrane (a), and cross section view of $Co_{73}Cu_{27}$ nanowires inside the pores clearly observed in light grey contrast (b).*

Transmission electron microscopy (TEM) studies were carried out in a FEI-TITAN 80-300 kV microscope operated at 300 kV in both TEM and STEM (scanning transmission electron microscopy) modes. In this case, Co-Cu nanowires were released from the PAAMs templates, dispersed in ethanol-distilled water mixture (1:1) and sonicated during 10 minutes at room temperature. Then, a drop of the resulting suspension was placed onto a lacey-carbon gold grid and the solvent was evaporated in ambient environment. In TEM mode, the images were acquired in a CCD Gatan camera with 1K digital resolution. For STEM mode, the images were registered using the high angle annular dark field detector (HAADF-STEM) which, together with the energy dispersive X-ray spectroscopy (EDS), allows us to determine the distribution of each element in Co-Cu nanowires. The strong sensitivity of this technique to the atomic number of the element allows us to mapping with compositional contrast of the alloy. Fig. 2 shows a typical HAADF STEM image and EDS elemental mapping of both Co-Cu nanowires composition. As observed, both Co and Cu elements are locally rather uniformly distributed inside the nanowire core. Moreover, it can be assumed that the elements form an alloy, at least locally, since there is no evidence of any granular arrangement of Cu atoms immersed in the Co matrix, under the resolution of the elemental mapping measured by EDS and performed in STEM mode (in our case, less than 10 nm). However, the $Co_{92}Cu_8$ nanowire exhibits some regions where its relative composition is not homogeneous, which can affect to the overall magnetic behavior in this specific sample.

Structural characterization

The local atomic arrangement of Co can be modified by the addition of elements with a different crystalline symmetry. Since the Cu tends to crystallize in *fcc* structure, the incorporation of Cu into the Co structure is expected to favor the formation of Co-Cu alloys with the cubic structure. Figure 3 displays the XRD data performed with the nanowires embedded into the pores of the alumina templates. The XRD pattern of pure Co nanowire arrays shown in the upper panel of Figure 3, shows the coexistence of both *hcp* and *fcc* phases. In the case of the *hcp* crystalline structure, the high intensity of the peaks related to the reflections $(100)_{hcp}$ and $(110)_{hcp}$ together with the absence of the main $(101)_{hcp}$ peak characteristic of the *hcp* phase suggests the existence of a strong texture in the Co crystals having their c-axis nearly perpendicular to the nanowires axis[34].

For small Cu content, the $(110)_{hcp}$ or $(220)_{fcc}$ reflections disappear, while the $(200)_{fcc}$ is now observed, indicating that the addition of Cu also affects to the crystalline texture of the nanowires. Furthermore, the relative change in the intensity of $(100)_{hcp}$ peak observed in Co-Cu nanowires when increasing the amount of Cu content in the alloy, has been ascribed to a change in the crystalline texture of these nanowires, which can be modified not only due to the increasingly addition of Cu into the Co structure, but also the confined growth of the alloyed nanowires inside the parallel aligned nanochannels of the alumina template. Nevertheless, a complete quantitative estimation on the relative amount of each crystalline phase is rather difficult to obtain owing to the strong observed texture.

	Lattice parameter (Å)		
	[100]-hcp	[002]-hcp	[111]-fcc
Co	2.503	4.1250	3.535
$Co_{92}Cu_8$	2.505	4.0343	3.542
$Co_{73}Cu_{27}$	2.511	4.0374	3.549

Table 1: *Length of the lattice parameters, obtained from the XRD data, along different directions of both hcp and fcc crystalline phases, as a function of the Cu content in the Co-Cu alloy nanowires.*

These data indicate the coexistence of both *hcp* and *fcc* phases and that the nanowire arrays exhibit a strong crystalline texture related to the well-ordered alignment of the nanowires inside the nanoporous alumina templates, and their tendency of growing with the $[100]_{hcp}$ direction along the nanowires length, being the c-axis nearly perpendicular to the nanowire axis. Moreover, the increasingly incorporation of Cu into the nanowires structure favors this texture and leads to a slight shift of the $(100)_{hcp}$ and $(002)_{hcp}$ peaks to lower and higher angles, respectively, (having 2θ values of 41.627(2)°, 41.596(2)° and 41.492(1)°), suggesting that Cu atoms substitute some Co sites resulting in a deformation of the *hcp*-Co structure. This shift corresponds to a volume compression along the $[002]_{hcp}$ direction and expansion along the $[100]_{hcp}$ one, together an increase of the lattice cell parameter *a* of the *fcc* crystalline structure, as can be seen in Table 1. The mean structural coherence lengths associated to the $(100)_{hcp}$ peaks, L_{100}, corresponding to the three samples were estimated from the full

View Article Online
DOI: 10.1039/C4TC02988G
Journal Name

width at half maximum (FWHM) of these peaks through the Scherrer equation[35]. The estimated values for the crystal size of the *hcp* phase in the [100] direction were 285, 507 and 288 nm for the pure Co, $Co_{92}Cu_8$ and $Co_{73}Cu_{27}$ nanowire arrays, respectively.

For a more accurately determination of the crystalline orientation, high resolution transmission electron microscopy (HR-TEM) and selected area electron diffraction (SAED) measurements have been carried out in $Co_{92}Cu_8$ and $Co_{73}Cu_{27}$ single nanowires, whose TEM images are displayed in figures 4 a) and 4 d), respectively. The SAED patterns were interpreted with simulations of the Web-based Electron Microscopy Application Software: Web-EMAPS[36].

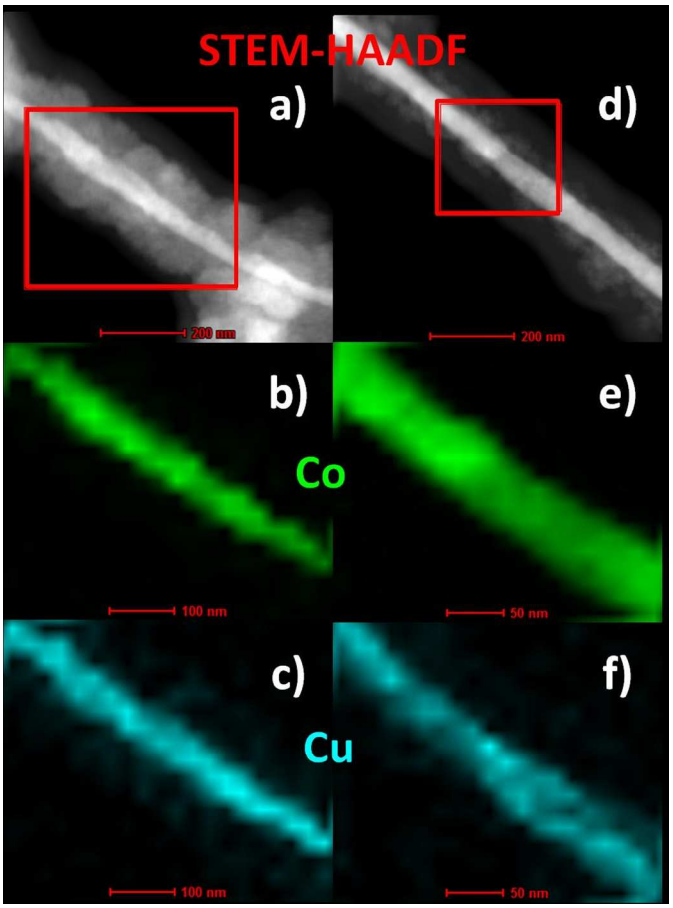

Figure 2: *a) Micrograph of a $Co_{73}Cu_{27}$ nanowire obtained by STEM operated in HAADF mode. Elemental mapping of the same nanowire region shows the spatial distribution of b) Co and c) Cu, respectively. Images d), e) and f) display the respective corresponding studies performed in a $Co_{92}Cu_8$ nanowire.*

The electron diffraction patterns of different nanowire regions confirmed the coexistence of *hcp* and *fcc* crystalline structures in both Co-Cu samples. Typical SAED patterns are presented in Figures 4 b) and 4 e) for the respective nanowires. Figure 4 b) shows the SAED pattern of an isolated $Co_{92}Cu_8$ nanowire, whose corresponding TEM image is presented in Figure 4 a). Such pattern consists of slightly elongated spots, suggesting the presence of several crystals with the same crystalline phase but slightly deviated orientations. This pattern can be indexed to the [110] zone axis of a *fcc* phase of Co (or Co-Cu). It was found that the <111> direction lies close to the nanowire axis, with a deviation angle of 7°. Figure 4 c) shows a dark field TEM image obtained using the reflection (1-1-1). In this image several crystalline domains are observed (in white) confirming the polycrystalline nature of the nanowires. Figure 4 e) corresponds to the SAED pattern obtained from a segment of a $Co_{73}Cu_{27}$ single nanowire, whose TEM micrograph is presented in Figure 4 d). This pattern can be associated to the [111] zone axis of an *hcp* phase of Co (or Co-Cu).

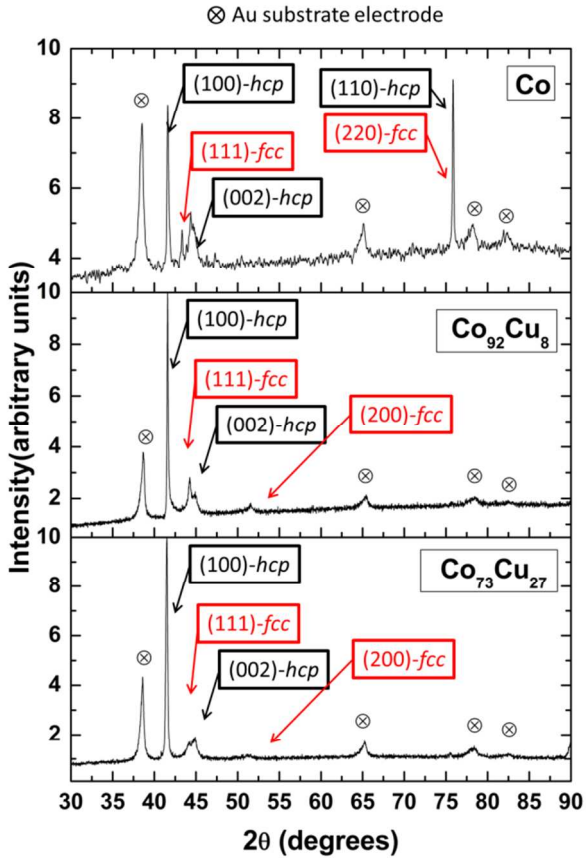

Figure 3: *XRD patterns for Co (upper panel), $Co_{92}Cu_8$ (middle) and $Co_{73}Cu_{27}$ (bottom), where the Co or Co-Cu reflections corresponding to the fcc and hcp phases are highlighted in red and black, respectively.*

Interestingly, the crystallographic <100> direction roughly points along the nanowire axis; however this pattern presents several remarkable peculiarities. In concrete, it is constituted by spots that tend to accumulate forming "short lines" denoting the presence of several nanocrystals sharing the same crystallographic directions (the estimated maximum deviation angle is 26.7°, as observed in Figure 4 e)). It is striking that these short lines forming the spots are not concave with respect to the center of the pattern (as it would be expected for several single crystals imperfectly attached in an oriented way), but appear straight or even convex with respect to the center of the pattern. This indicates the presence of oriented lattice distortions in the attached crystals, probably produced by the Cu incorporation into the Co structure. Figure 4 f) depicts a dark field TEM image obtained using the reflection (0-11)

Journal Name

View Article Online
DOI: 10.1039/C4TC02588G ARTICLE

where several crystalline domains are observed. These results lead us to conclude that the uniform insertion of Cu atoms in the Co structure has been achieved. Such insertion induces distortions in the crystal lattice favoring the formation of *hcp* crystals attached with their [1-10] direction along the axis of the nanowires. Moreover, these distortions also favor the presence of *fcc* crystals oriented with the [111] direction along the nanowire axis.

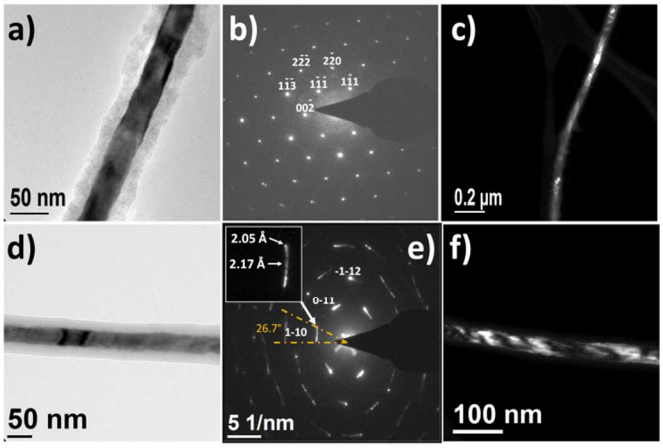

Figure 4: *a) TEM micrograph of a region of an isolated $Co_{92}Cu_8$ nanowire. b) SAED pattern obtained for the nanowire segment of image a). c) (1-1-1) dark-field TEM image of the same nanowire as in b). d) TEM micrograph of a segment of a $Co_{73}Cu_{27}$ single nanowire. e) SAED pattern obtained for the nanowire segment of image d). f) (0-11) dark-field TEM image of the same nanowire as in e).*

MAGNETIC BEHAVIOR

Room temperature hysteresis loops (HLs) of the samples have been measured in a Vibrating Sample Magnetometer (KLA-Tencor EV7) under maximum applied magnetic field of ±1.5T as a function of the angular orientation of the applied field from parallel to perpendicular direction with respect to the nanowires axis. The temperature dependent measurements were measured in a VSM-Versalab (Quantum Design) in parallel and perpendicular configurations of the applied magnetic field, in the range of 50-400 K under a maximum applied magnetic field of ±3T.

Hysteresis loops at room temperature.

The HLs measured at room temperature are shown in Fig. 5a). A first rough comparative analysis of the parallel and perpendicular loops indicates a clear anisotropic behavior indicating an overall magnetic anisotropy along the axis of the nanowires although a more detailed angular analysis is conducted later. We also observe that the presence of Cu leads to an increase of axial coercivity from 863 Oe in pure Co nanowire array up to 1474 Oe in $Co_{73}Cu_{27}$ one, while the $Co_{92}Cu_8$ sample shows the intermediate value of 1396. Interpretation of that increase is not straightforward since Cu content reduces proportionally the saturation magnetization of the samples and consequently the corresponding shape anisotropy and the magnetostatic interactions. In addition, the introduction of Cu in the alloy can originate local defects, such as dislocations and twin boundaries[37], serving as pinning centers for the walls displacement.

Taking into account the structural analysis for pure Co nanowires in the previous section, the presence of the *hcp* c-axis perpendicular to the nanowires axis should result in a competition between shape and magneto-crystalline anisotropies[34]. On the other hand, the presence of the *fcc* phase in pure Co nanowires is reinforced as the Cu content increases. Owing to the weaker crystalline anisotropy constant of that *fcc* phase, the shape anisotropy promotes a net parallel magnetic anisotropy in Cu enriched alloys.

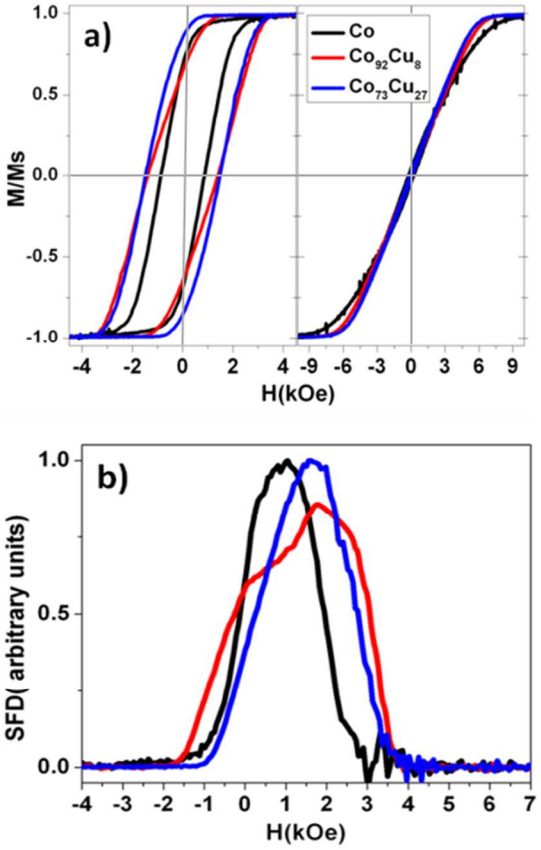

Figure 5: *a) Room temperature hysteresis loops with the magnetic field applied parallel (left), and perpendicular (right) to the nanowires axis for indicated samples. b) Switching field distribution obtained from the HL in a) for pure Co (black), $Co_{92}Cu_8$ (red) and $Co_{73}Cu_{27}$ (blue) nanowire arrays.*

We should also mention the particular behavior of $Co_{92}Cu_8$ nanowire array which exhibits a change in the magnetic susceptibility at a parallel field near the coercivity. If we pay attention on the descendant branch of the corresponding parallel HL of Figure 5 a), the magnetization leaves the saturation nearly following the pure Co sample HL, and approaches that of the $Co_{73}Cu_{27}$ sample close to the coercivity. That change of the susceptibility can be analyzed in terms of the presence of two magnetic phases. The softer magnetic phase, which reverses its magnetization first, could be ascribed to the pure Co nanowire array and the harder magnetic phase to the high Cu content nanowire array. That behavior is also supported even more clearly on the Switching Field Distribution (SFD), obtained here as the first derivative of the ascendant branch of the HL, and represented in Figure 5 b). The SFD of the $Co_{92}Cu_8$ nanowire array can be represented by the superposition of the two SFDs corresponding to pure Co and $Co_{73}Cu_{27}$-like magnetization reversal behaviors, as can be seen in the

ARTICLE View Article Online
DOI: 10.1039/C4TC02988G Journal Name

contributions of two peaks centered at around 1 kOe and 2 kOe, respectively. Apparently, the presence of the two magnetic phases cannot be directly ascribed to the hcp and fcc crystalline structures since the mixture of crystalline phases is observed in all samples.

Magnetic characterization based in First Order Reversal Curves (FORC).

The FORC analysis has been widely employed in the study of the magnetization reversal processes in magnetic nanowire arrays[38]. It assumes that the major hysteresis loop is composed by the superposition of elementary magnetization reversal processes called hysterons. Each hysteron displays a squared shaped loop characterized by a coercivity (H_c), and an interaction field (H_u) which represents the shift of the complete hysteron with respect the zero field axis and commonly ascribed to the magnetostatic interactions among nanowires. As the hysterons are magnetically bistable, the coercive field and the switching field values at which the reversal of the magnetization occurs are the same. Since FORC analysis enables to extract the magnetostatic interactions among nanowires, the estimation of the switching field of all the hysterons through the FORC analysis is translated in the estimation of the intrinsic SFD[39,40].
Figure 6 shows the results of the FORC analysis for the arrays of Co-Cu nanowires parallel magnetized to their axes. In the case of Co and $Co_{73}Cu_{27}$ nanowire arrays (Figure 6 a) and 6 c), respectively), FORC diagrams exhibit a typical "wishbone" shape characteristic of arrays of interacting magnetic nanowires[41]. The main difference between them has already been displayed in the HL, i.e., the harder magnetic behavior of the $Co_{73}Cu_{27}$ nanowires. The mean coercive field values, H_C^{forc}, extracted from the FORC diagrams are 826 Oe and 1513 Oe for Co and $Co_{73}Cu_{27}$ nanowire arrays, respectively, fitting with the values extracted from the HLs. However, this is the only significant difference between them since the standard deviation of the SFDs, as well as the strength of the interaction field at saturation (α) are very similar in both cases, around 260 Oe and 1650 Oe, respectively. Therefore, it seems reasonable to think that such parameters are mainly ascribed to the specific characteristics of the patterned alumina templates that match the nanowires grown inside the pores of the alumina membranes. In the first case, the standard deviation could be due to a pore size distribution produced during the anodization of the patterned alumina templates

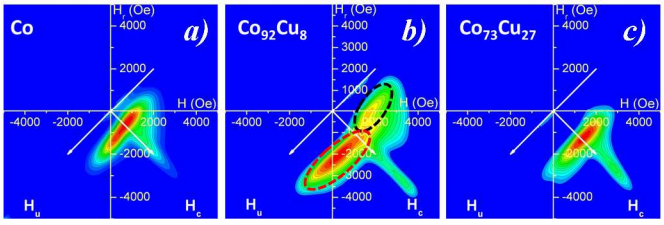

Figure 6: *FORC diagrams corresponding to parallel applied field configuration for a): Co; b): $Co_{92}Cu_8$ and c): $Co_{73}Cu_{27}$ nanowire arrays.*

The FORC diagram shown in Figure 6 b) for the $Co_{92}Cu_8$ sample displays a more complex magnetic behavior where two different but close to each other distributions are clearly observed. The main distribution, highlighted in red, is centered at the same value of coercive field as for the $Co_{73}Cu_{27}$ sample, while the other one highlighted in black corresponds to the coercive field of the Co nanowire array. The fact that both distributions are shifted along the interaction field axis suggests that both magnetic phases are interacting between them. Furthermore, the FORC diagram for the $Co_{92}Cu_8$ sample is not a result of the superposition of the Co and $Co_{73}Cu_{27}$ FORC diagrams. Neither the individual FORC distributions keep their shape, i.e., they are not only shifted by the interaction field but rather the distribution shape is modified suggesting that additional magnetic effects are taking place. As it was already shown by the room temperature HLs, $Co_{92}Cu_8$ sample presents two different ferromagnetic behaviors. Taking into account the fabrication process, significant differences among neighbor nanowires into the array are not expected, thus concluding that the nanowires are composed by a mixture of hard and soft magnetic phases. As it has been extracted from the HL and FORC analysis the harder magnetic phase is related to high Cu content. However, the magnetic hardening of the HL, or in other words, the large contribution to the magnetization of the harder magnetic phase with as low Cu concentration as 8 at.% is somehow surprising. This effect can be explained assuming that the harder magnetic phase pins the magnetization of the softer one leading in a major HL more similar to the harder magnetic behavior, such as in the case of $Co_{73}Cu_{27}$ HL, but even with such small amount of Cu into the alloy. Furthermore, this effect should depend on the relative difference between the switching fields of softer and harder magnetic phases.
Since the temperature dependence of the magnetic behavior of each phase is expected to be different, we have proceeded to the measurements of HLs at different temperatures.

Temperature dependence of magnetization process.

Figure 7 shows the temperature dependence of coercivity (H_c) and normalized remanence (m_R) of Co-Cu nanowire arrays for the parallel field configuration. An overall increase of both coercivity and remanence with increasing temperatures is observed, which leads to assume an increase of the effective magnetic anisotropy with the easy axis lying along the nanowire axis. Nevertheless, each sample shows significant differences for example in the evolution of coercivity. For Co nanowires there is a critical temperature at around 180 K at which coercivity changes the trend. For $Co_{92}Cu_8$ coercivity increases monotonically with temperature and shows the highest absolute variation.
The origin for the temperature dependence of coercivity in each case should reflect the compromise of the temperature dependence for all the magnetic anisotropy energy contributions namely, magnetoelastic, magnetocrystalline and shape or magnetostatic terms.
Regarding the magnetoelastic anisotropy term, there are two contributions, the temperature dependence of the magnetostriction constants and that one of the mechanical stresses arising from the different thermal expansion coefficients of metallic nanowires and ceramic alumina template. On cooling, the metallic nanowires tend to contract faster than the ceramic alumina so giving rise to radial tensile mechanical stress. If we consider the negative sign of the magnetostriction coefficient for polycrystalline Co ($\lambda_S \sim -62 \times 10^{-6}$), those stresses would result in increasing uniaxial anisotropy parallel to the nanowires in opposition to what we observe experimentally. As reported elsewhere, the magnetostriction contribution is not strong enough to justify a significant increase of magnetoelastic anisotropy when reducing the temperature[30-32].

Journal Name

View Article Online
DOI: 10.1039/C4TC02588G ARTICLE

Since the Curie Temperature of Co takes an elevated value of 1388K[42], appreciable differences on the saturation magnetization in the range of 50-300 K are not expected, thus suggesting a negligible temperature dependence of the shape anisotropy. This is the main reason why the magnetocrystalline anisotropy seems to play a more relevant role, and even it has been proposed to be responsible of the temperature reorientation of the effective magnetic anisotropy in Co-based nanowires[43,44].

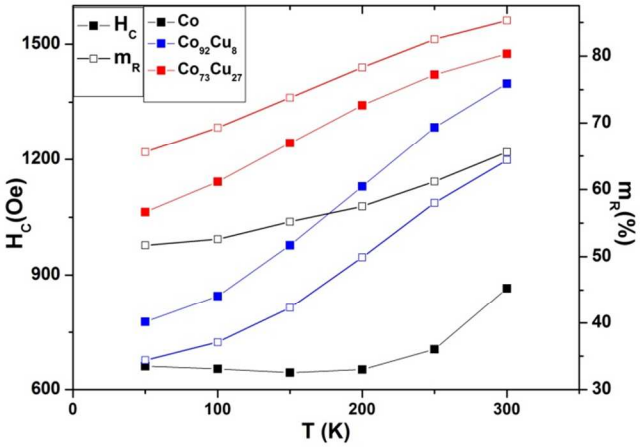

Figure 7: *Temperature dependence of parallel coercivity H_c (close squares) and $m_r(\%)=(M_r/Ms)\times100$ (open squares) for Co (black), $Co_{92}Cu_8$ (blue) and $Co_{73}Cu_{27}$ (red) nanowire arrays.*

It is important to note that the largest variations of H_C and m_r with temperature are observed in the $Co_{92}Cu_8$ nanowires sample, which presents the coexistence of two ferromagnetic phases (blue data in Figure 7). The temperature dependence of each ferromagnetic phase can be distinguished analyzing the upper branch of the major HL shown in Figure 8. In terms of the saturation field, defined as the minimum field required to nearly saturate the magnetic material along a given direction, Figure 8 b) shows that, for Co nanowire array, the easy magnetization axis tends to rotate from the parallel direction to the nanowire axis, at room temperature, to the perpendicular one at lower temperatures since the saturation field decreases with increasing temperatures.

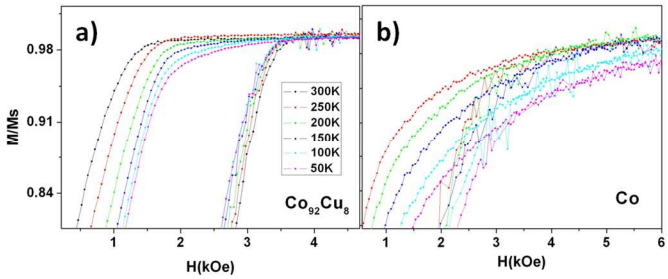

Figure 8: *Detail of the magnetization at the high-field region of major hysteresis loops measured at different temperatures for $Co_{92}Cu_8$ (a), and pure Co (b) nanowire arrays.*

Figure 8 a), which is related to $Co_{92}Cu_8$ sample, requires of more detailed explanation since different magnetization processes are observed. As it was mentioned above, the sample corresponding to $Co_{92}Cu_8$ composition presents magnetically softer and harder behaviors associated to pure Co and Co-Cu ferromagnetic phases, respectively. Taking a look to the upper part of the hysteresis loop, it can be deduced that the ascendant branch shows the harder magnetization reversal processes, here related to a pure Co-Cu magnetic phase. On the other hand, the descendant branch of HL corresponds to first reversals processes, which are those corresponding to the magnetically softer phase and thus ascribed to the pure Co like magnetic phase. For this reason, the Figure 8 a) reveals the temperature dependence of the two different magnetic phases by separately, where each branch of the upper region of HL can be correlated with the magnetic behavior of each ferromagnetic phase. First, it is interesting to note that the ascendant branch of the HLs of Figure 8 a) does not show a significant temperature dependence, that allows us to conclude that the switching field related to the harder (high Cu content) magnetic phase is almost constant. However, the descendant branch of the HLs in the same figure, which is related to the softer (pure Co) magnetic phase, shows the highest temperature dependence by decreasing its mean switching field, i.e. is getting magnetically softer, as the temperature decreases.

In summary, we can conclude that the switching field of the harder magnetic phase remains nearly constant with temperature, while that one for the softer magnetic phase decreases with temperature decreasing. This last fact supports the assumption of the presence of two different magnetic contributions in $Co_{92}Cu_8$ nanowire array coming from a pure Co-like (softer) and $Co_{73}Cu_{27}$-like (harder) magnetic phases. It is worth noting that in Figure 7, the coercive field dependence on temperature for the $Co_{92}Cu_8$ sample shows that at room temperature, the largest contribution comes from the harder magnetic phase, similar to the coercive field of the $Co_{73}Cu_{27}$ one, whilst reducing the temperature, the coercive field is more influenced by the softer magnetic phase of pure Co. Then, the total temperature variation of the $Co_{92}Cu_8$ is not only influenced by the intrinsic temperature dependence of pure Co nanowires but rather by the presence of the two different ferromagnetic phases.

Magnetization reversal process as deduced from analytical calculations.

According to previous studies, three main idealized modes of magnetization reversal process have been identified in nanowire arrays: coherent rotation, with all the spins rotating simultaneously; transverse wall, in which spins reverse progressively via propagation of a transverse domain wall; and the vortex wall, in which spins reverse progressively via propagation of a vortex (curling) domain wall. All these modes result in different angular dependence of coercivity and they have been successfully employed, making use of the equations derived in references from elsewhere[45,46], to identify the specific magnetization reversal mechanism that better fits to experimental findings.

Figure 9 illustrates the experimental results for the three samples together with the calculated data according to the three different reversal modes. As observed, in all cases the magnetization reversal is driven by the nucleation and propagation of a transverse domain wall. That allows to conclude that the presence of Cu does not change the magnetization reversal mechanism but increases the absolute value of coercivity.

The values of the magnetocrystalline anisotropy, K_{mc}, used in the calculations to obtain the best agreement with experimental results, (-3.7×10^4 , 2.1×10^4 and 3.3×10^4 J/m^3 for Co, $Co_{92}Cu_8$ and $Co_{73}Cu_{27}$, respectively), point out once more the

View Article Online
DOI: 10.1039/C4TC02988G
Journal Name

contribution of the magnetocrystalline anisotropy to the reorientation of the effective magnetic anisotropy as a result of the amount of Cu present in the Co-Cu alloy. From these values, we observe that the easy axis of the magnetocrystalline anisotropy evolves from perpendicular direction in the case of Co nanowire arrays (corresponding to negative values of K_{mc}), toward parallel aligned with respect to the nanowires axis in the case of Cu-rich alloys (positive values of K_{mc}). However, the shape anisotropy is still dominant and the effect of the change in the sign of K_{mc} is to make decrease slightly the effective magnetic anisotropy in the case of pure Co nanowire array.

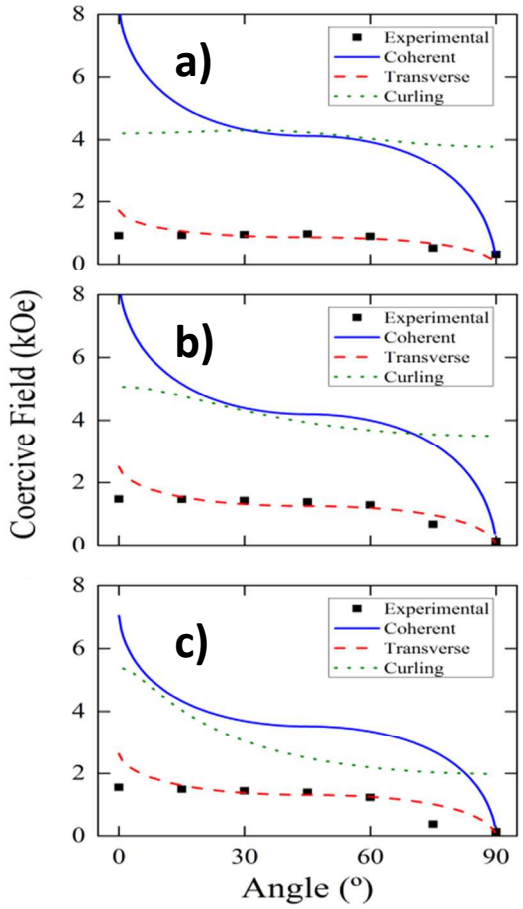

Figure 9: *Experimental and calculated coercivity dependence on the angle between the applied magnetic field and the nanowires axis, for a) Co; b) $Co_{92}Cu_{08}$ and c) $Co_{73}Cu_{27}$ nanowires.*

This fact points out the influence of Cu addition over the crystalline structure as it was already discussed in the structural section. However, we should also mention that the model does not consider magnetostatic interactions among neighboring wires, which could justify the lack of perfect fitting.
Nevertheless, under the mean field interaction theory, the coercive field of the nanowire array should not be affected, since the interaction field is supposed to be proportional to the magnetization, which validates the application of the analytical calculation in this kind of systems. It is worth also to mention that, as we are dealing with the coercivity of the whole nanowire array, the presence of the two magnetic phases in the $Co_{92}Cu_8$ sample makes the coercive field differing from the switching field of the nanowires, starting to be a magnetic configuration that depends on the relative amount between each ferromagnetic phase.

Summary and Conclusions

Co and Co-Cu alloy nanowire arrays have been potentiostatically electrodeposited into the spatially self-ordered pores of anodic alumina templates. By $CuCl_2$ addition to the Co Watts-type electrolyte and varying the electrodeposition voltage, the amount of Cu into the Co-Cu nanowires has been properly tuned in the range between 0 up to 27 at.%. Co nanowires present a mixture of *fcc* and *hcp* crystalline phases, being the last one the main phase with its c-axis lying along the perpendicular direction with respect to the nanowire axis. However, the presence of Cu modifies its crystalline texture. TEM/SAED and EDS characterization have corroborated the XRD results and pointed out that Cu is homogeneously distributed along the entire nanowire.
Hysteresis loops indicate that all the nanowire arrays present a well-defined uniaxial effective magnetic anisotropy with the easy magnetization axis lying parallel to the nanowires axis. From comparison among the corresponding hysteresis loops for the different Co-Cu alloy nanowire arrays, the coercive field and squareness both increase as the amount of Cu increases, being the nanowires more sensitive to the shape anisotropy. Furthermore, the nanowire arrays having lower amount of Cu composition, namely the $Co_{92}Cu_8$ sample, presents two clearly different irreversible magnetization reversal processes, which suggest that two ferromagnetic phases are present in the sample. In addition, the magnetically softer phase would correspond to a pure-Co-like nanowire array, whilst the harder one could be ascribed to a Co-Cu phase. FORC measurements have also displayed two different irreversible magnetization reversal processes in the case of the $Co_{92}Cu_8$ nanowire array. But in principle, the resulting FORC diagram does not correspond with two independent SFDs, suggesting that additional interaction effects between both ferromagnetic phases play an important role in the magnetic behavior of this sample. The increase of both, the coercive field and reduced remanence with increasing temperatures has been ascribed, according to the literature, to a reduction of the magneto-crystalline anisotropy of Co-*hcp* phase as the temperature is increased, promoting a higher uniaxial effective magnetic anisotropy. However, as far as the *hcp* phase is reduced with the addition of Cu, it is in principle peculiar that the strongest effect of temperature on the coercive field and remanence has been found in the $Co_{92}Cu_8$ nanowire array, where the two different ferromagnetic phases coexist. Thus the temperature dependence of coercivity could be increased by a change in the interaction features, which could be affected by the differences between switching fields associated to each ferromagnetic phase. Finally, it is clear the need of controlling the exact amount of Cu addition in the ferromagnetic layer of multilayered systems in order to avoid different ferromagnetic phases coexistence or tune the magnetic properties of each layer.

Acknowledgements

Financial support of Spanish MICINN under research projects Nº MAT2010-20798-C05-01 and 04, and MINECO research Projects Nº MAT2013-48054-C2-1-R and 2-R, and MAT2013-47231-C2-1-P are gratefully acknowledged. Mexican funding from the Mexican Council of Science and Technology

View Article Online
DOI: 10.1039/C4TC02588G

(CONACYT), and Universidad Autónoma de Nuevo León under research projects CB12-179486 and PAICYT-CE793-11, respectively, is also acknowledged. J. García thanks to FICYT for a ''Severo Ochoa'' fellowship. Scientific support from the University of Oviedo SCT's, particularly to the *Laboratorio de Membranas Nanoporosas* at Nanotechnology Unit, is also recognized.

Notes and references

[a]*Depto. de Física, Universidad de Oviedo, Calvo Sotelo s/n, 33007-Oviedo, Asturias, Spain*
[b]*Instituto de Ciencia de Materiales de Madrid, ICMM-CSIC, 28049-Madrid, Spain*
[c]*Centro de Investigación en Ciencias Físico Matemáticas (CICFiM), Facultad de Ciencias Físico-Matemáticas (FCFM), Universidad Autónoma de Nuevo León (UANL), Av. Pedro de Alba s/n, San Nicolás de los Garza, 66450-Nuevo León, Mexico*
[d]*Facultad de Ingeniería Mecánica y Eléctrica (FIME), Universidad Autónoma de Nuevo León (UANL), Av. Pedro de Alba s/n, San Nicolás de los Garza, 66450-Nuevo León, Mexico*
[e]*Depto de Física, Universidad de Santiago de Chile (USACH), and Center for the Development of Nanoscience and Nanotechnology (CEDENNA), Avda. Ecuador 3493, Santiago, Chile*

1 S. Da Col, S. Jamet, N. Rougemaille, A. Locatelli, T. O. Mentes, B. Santos Burgos, R. Afid, M. Darques, L. Cagnon, J. C. Toussaint, and O. Fruchart, *Phys. Rev. B*, 2014, **89**, 180405(R).
2 H. Forster, T. Schrefl, D. Suess, W. Scholz, V. Tsiantos, R. Dittrich, and J. Fidler, *J. Appl. Phys.*, 2002, **91**, 6914.
3 S. Sun, C. B. Murray, D. Weller, *Science*, 2000, **287**, 1989.
4 Q. F. Liu, C. X. Gao, J. J. Xiao, and D. S. Xue, *J. Magn. Magn. Mater.,* 2003, **260**, 151.
5 P. Schio, F. J. Bonilla, Y. Zheng, D. Demaille, J. Milano, A. J. A. de Oliveira, and F. Vidal, *J. Phys Condens. Matter.*, 2013, **25**, 056002.
6 M. Darques, L. Piraux, A. Encinas, P. Bayle-Guillemaud, A. Popa, and U. Ebels, *Appl. Phys. Lett.*, 2005, **86**, 072508.
7 L. G. Vivas, J. Escrig, D. G. Trabada, G. A. Badini-Confalonieri, and M. Vázquez, *Appl. Phys. Lett.*, 2012, **100**, 252405.
8 J. U. Cho, J. H. Wu, J. H. Min, S. P. Ko, J. Y. Soh, Q. X. Liu, and Y. K. Kim, *J. Magn. Magn. Mater.*, 2006, **303**, e281-e286.
9 X. Liu, J. Zhao, Y. Li, S. Xu, Z. Zhu, J. Chen, and G. Wu, *Chem. Lett.*, 2007, **36**, 166-167.
10 V Vega, T Böhnert, S Martens, M Waleczek, J M Montero-Moreno, D Görlitz, V M Prida, and K Nielsch, *Nanotechnology*, 2012, **23**, 465709.
11 C. Bran, Yu. P. Ivanov, D. G. Trabada, J. Tomkowicz, R. P. del Real, O. Chubykalo-Fesenko, and M. Vazquez, *IEEE Trans. Magn*., 2013, **49**, 4491.
12 T. Nishizawa, and K. Ishida, *Bulletin of Alloy Phase Diagrams*, 1984, **5**, 161-165.
13 A. E. Berkowitz, J. R. Mitchell, M. J. Carey, A. P. Young, S. Zhang, F. E. Spada, F. T. Parker, A. Hutten, and G. Thomas. *Phys. Rev. Lett*., 1992, **68**, 3745.
14 J. Q. Xiao, J. S. Jiang, and C. L. Chien, *Phys. Rev. Lett*., 1992, **68**, 3749.
15 H. Zaman, A. Yamada, H. Fukuda, and Y. Ueda, *J. Electrochem. Soc*., 1998, **145**, 565-568.
16 Ö. F. Bakkaloglu, and I. H. Karahan, *Turk. J. Phys*., 2001, **25**, 27-33.
17 M. Almasi Kashi, A. Ramazani, and F. Adelnia Najafabadi, *J. Alloys Compd*., 2012, **540**, 133-136.
18 P. R. Evans, G. Yi, and W. Schwarzache, *Appl. Phys. Lett*., 2000, **76**, 481-483.
19 P. Y. Chen, S. F. Hu, C. Y. Huang and R. S. Liu, *J. of Electromagn. Waves and Appl*., 2010, **24**, 1609-1620.
20 D. Pullini, and D. Busquets Mataix, *ACS Appl. Mater. Interfaces*, 2011, **3** (3), 759–764.
21 D. Pullini, G. Innocenti, D. Busquets, and A. Ruotolo, *Appl. Phys. Lett.,* 2007, **90**, 133106.
22 D. Pullini, D. Busquets, A. Ruotolo, G. Innocenti, and V. Amigó, *J. Magn. Magn. Mater*., 2007, **316** (2), e242-e245.
23 D. Pullini, D. Busquets Mataix, and A. Tommasi, *Co/Cu Nanowire Systems for GMR Sensing Applications, Nanowires - Implementations and Applications*, 2011, Abbass Hashim (Ed.), ISBN: 978-953-307-318-7, InTech.
24 A. Mourachkine, O. V. Yazyev, C. Ducati, and J.-Ph. Ansermet, *Nano Lett.*, 2008, **8** (11), 3683-3687.
25 T. Böhnert, A. C. Niemann, A.-K. Michel, S. Bäßler, J. Gooth, B. G. Tóth, K. Neuróhr, L. Péter, I. Bakonyi, V. Vega, V. M. Prida, and K. Nielsch, *Phys. Rev. B*, 2014, **90**, 165416.
26 O. Karaagac, M. Alper, and H. Kockar, J. Magn. Magn. Mat., 2010, **322**, 1098-1101.
27 M. A. Kashi, A. Ramazani, F. A. Najafabadi, and Z. Heydari, *Appl. Surf. Sci*., 2011, **257**, 9347-9350.
28 Z. H. Yang, Z. W. Li, L. Liu, and L. B. Kong, *J. Magn. Magn. Mat*., 2011, **323**, 2674-2677.
29 E. Köster, *Phys. Status Solidi (b)*, 1968, **30**, 455–460.
30 D. Navas, K. R. Pirota, P. Mendoza Zelis, D. Velazquez, C. A. Ross, and M. Vazquez, *J. Appl. Phys.,* 2008, **103**, 07D523.
31 M. Vázquez, K. Pirota, J. Torrejón, D. Navas, and M. Hernández-Vélez, *J. Magn. Magn. Mater*., 2005, **294**, 174-181.
32 A. K. Srivastav, and R. Shekhar, *J. Magn. Magn. Mat*., 2014, **349**, 21-26.
33 H. Masuda, and K. Fukuda, *Science,* 1995, **268**, 1466.
34 K. Maaz, S. Karim, M. Usman, A. Mumtaz, J. Liu, J. L. Duan and M. Maqbool, *Nanoscale Res. Lett.*, 2010, **5**, 1111-1117.
35 B. D Cullity, and S. R. Stock, *Elements of X-ray Diffraction*, 3rd ed.; 2001, Prentice Hall: Upper Saddle River, NJ.
36 J. M. Zuo, and J. C. Mabon, *Microsc. Microanal*. 2004, **10** (Suppl 2), URL: http://emaps.mrl.uiuc.edu/.
37 W. Liang, and M. Zhou, *Nano Lett.*, 2005, **5** (10), 2039-2043.
38 F. Béron, L. P. Carignan, D. Ménard, and A. Yelon, *Electrodeposited Nanowires and their Applications, Chapter 7*, 2010, ISBN: 978-953-7619-88-6.
39 F. Béron, D. Ménard, and A. Yelon, *J. Appl. Phys*., 2008, **103**, 07D908.
40 I. D. Mayergoyz, "Mathematical Models of Hysteresis", 1991, Springer-Verlag: New York.

View Article Online
DOI: 10.1039/C4TC02988G
Journal Name

41 C. R. Pike, C. A. Ross, R. T. Scalettar, and G. Zimanyi, *Phys. Rev. B*, 2005, **71**, 134407.
42 P. Heller, *Rep. Prog. Phys*., 1967, **30**, 731.
43 H. B. Callen, and E. Callen, *J. Phys. Chem. Solids*, 1966, **27**, 1271–1285.
44 E. L. Silva, W. C. Nunes, M. Knobel, J. C. Denardin, D. Zanchet, K. Pirota, D. Navas, and M. Vázquez, *Physica B*, 2006, **384**, 22–24.
45 R. Lavín, J. C. Denardin, J. Escrig, D. Altbir, A. Cortés, and H. Gómez, *J. Appl. Phys*., 2009, **106**, 103903.
46 J. Escrig, R. Lavin, J. L. Palma, J. C. Denardin, D. Altbir, and A. Cortes, H. Gomez, *Nanotechnology*, 2008, **19**, (2008) 075713.